

IS IGR J17091-3624 A MISSING LINK BETWEEN GRS 1915+105 AND OTHER BLACK HOLE LOW MASS X-RAY BINARIES?

Mayukh Pahari¹, J S Yadav¹ and Sudip Bhattacharyya¹

¹ *Tata Institute of Fundamental Research, Homi Bhabha Road, Mumbai, India; mp@tifr.res.in*

ABSTRACT

In this work, we study the timing and spectral evolution of the transient low mass X-ray binary IGR J17091-3624 during its 2011 outburst. We present results obtained from observations with two instruments, *Rossi X-ray Timing Explorer (RXTE)* proportional counter array (PCA) and *SWIFT* X-ray telescope (XRT), between 03 February 2011 and 10 April 2011. Apart from the detection of increase in X-ray flux while moving from the canonical low hard state to the hard intermediate state, we report the details of a transition from a low irregular variability state, commonly seen from most of the black hole X-ray binaries (BHXBs), to a regular, repetitive and large variability state, seen only from GRS 1915+105 (ρ class variability). By comparing the timing and spectral properties of IGR J17091-3624 in the variable state with those of the ρ class of GRS 1915+105, we conclude that till now the former is the only known source, which somewhat behaves like GRS 1915+105, and could be used as a missing link between GRS 1915+105 and other canonical BHXBs in understanding their accretion and radiation mechanisms.

Subject headings: accretion, accretion disks — black hole physics — X-rays: observations — X-rays: binaries — X-rays: individual: (IGR J17091-3624, GRS 1915+105)

1. Introduction

IGR J17091-3624 was detected as a bright variable transient source, with flaring activity in October 1994 (Mir/KVANT/TTM), September 1996 (BeppoSAX/WFC), September 2001 (BeppoSAX/WFC; (In't Zand et al. 2003)), April 2003 (INTEGRAL/IBIS; Kuulkers et al. (2003)), and July 2007 (Capitanio et al. 2009). In April 2003, IBIS, the gamma-ray imager on board the *INTEGRAL* satellite detected the transient X-ray binary IGR J17091-3624 at the position of $17^h09.1^m$ (R.A. (J2000.0)), $-36^\circ24.63'$ (declination (J2000.0)) while monitoring the galactic centre (Kuulkers et al. 2003). A transition between soft and hard states and the presence of blackbody component during source softening were observed during a joint spectral analysis of *INTEGRAL*/IBIS and *RXTE*/PCA data by Capitanio et al. (2006). They found that the spectral behavior and time variability of the source was similar to the black hole candidate H1743-322. Lutovinov et al. (2003) found that the power density spectrum (PDS) of IGR J17091-3624 can be well described by

the standard model of band-limited noise with the break frequency of 0.31 ± 0.04 Hz and fitted the energy spectrum with the powerlaw model having powerlaw index of 1.43 ± 0.03 , commonly observed in X-ray binary systems in the low hard spectral state (Sunyaev & Revnivtsev 2000). *SWIFT*/XRT observations of IGR J17091-3624 during the outburst in 2007 revealed another state transition from hard to soft, and refined the X-ray position of this source, which was consistent with the position of a compact radio counterpart in the *VLA* archived data (Capitanio et al. 2009), as well as the position of the infrared counterpart observed with the *ESO New Technology Telescope* (NTT) (Chaty et al. 2008). Radio emission from this source with steep synchrotron emitting spectrum had been confirmed with the observations from the *Very Large Array* (VLA) (Rupen et al. 2003) and the *Giant Meterwave Radio Telescope* (GMRT) (Pandey et al. 2006). In spite of several efforts, little is known about the compact nature of this source. There is no optical observation of its binary counterpart. The renewed activity of the source was first detected by the *SWIFT*/BAT when the 15.0-50.0 keV hard X-ray flux increased upto 60 mCrab on 03 February 2011, compared its low hard level of ~ 10 mCrab (Krimm et al. 2011). This is next to the largest outburst (~ 70 mCrab) in 2007. Later using the *SWIFT*/XRT observation, Krimm & Kennea (2011) confirmed that the outburst occurred in the source IGR J17091-3624, and not in IGR J17098-3628, which is also an X-ray transient $9.6'$ away from IGR J17091-3624. The *INTEGRAL*/IBIS also detected the source simultaneously with the *SWIFT*/XRT (Del Santo et al. 2011). During 2011 outburst, the hard state activity of the source was detected with the IBIS/ISGRI imager and the JEM-X telescope on board the *INTEGRAL* satellite on 7–8 February, 2011 (Capitanio et al. 2011). They described the combined ISGRI and JEMX2 spectrum (5.0-300.0 keV) with a cut-off power law model with the high energy cutoff of 110^{+47}_{-27} keV.

From the beginning of the *RXTE* observations on 9 February 2011, several rich features and characteristics in timing and spectral domain of the source have been noticed. QPOs at 0.094 ± 0.003 Hz with a quality factor of ~ 9.1 , and at $0.105^{+0.004}_{-0.003}$ Hz with a quality factor of ~ 7.4 etc. were detected in the *RXTE*/PCA observations on 9, 10, 11 and 12 February, 2011 (Rodriguez et al. 2011a). Apart from this, fast QPO evolution (Shaposhnikov 2011), 10 mHz QPOs (Altamirano et al. 2011a) and evolving power density spectrum with multiple peaks (Pahari et al. 2011b) were also noticed. High frequency QPOs at 66 Hz (Altamirano & Belloni 2012) were detected with the significance of 8.5σ . Using Chandra spectroscopy of IGR J17091-3624, King et al. (2012) showed that accretion disk wind in soft, disk-dominated states, in apparent anti-correlation with relativistic jets in low hard state. This disk wind is observed to be highly ionized, dense, and has typical blueshift of ~ 9300 km/s or less projected along our line of sight. Lately, a quasi-regular oscillation in the lightcurve of IGR J17091-3624 was noticed which is very similar to the ‘ ρ ’ class variability seen only in the lightcurve of galactic microquasar GRS 1915+105 (Altamirano et al. 2011b). Later, Altamirano et al. (2011c) claimed few more variabilities similar to those found in GRS 1915+105. Two new variabilities which are unique to IGR J17091-3624 are reported by (Pahari et al. 2011a).

GRS 1915+105 is a Galactic microquasar which has shown spectacular X-ray variability since

its discovery in 1992 (Castro-Tirado et al. 1994). Out of 12 classes observed in the X-ray variabilities of GRS 1915+105 (Belloni et al. 2000), the ‘ ρ ’ class shows regular, repetitive bursts in the lightcurve with recurrence time between 40s and 110s. These recursive burst structures have been observed for extended duration and have been discussed by several authors (Taam et al. 1997; Paul et al. 1998; Yadav et al. 1999). Using the data from the Indian X-ray Astronomy Experiment (IXAE) onboard the Indian Satellite *IRS-P3* and *RXTE*, Yadav et al. (1999) found that these bursts which can be categorized as irregular, quasi-regular and regular bursts have a slow exponential rise and sharp linear decay. Using the *BeppoSAX* data, Massaro et al. (2010) concluded that the process responsible for the pulses produced strongest emission between 3.0 and 10.0 keV, and the emission at the rising phase of the pulse dominated the lower and higher energy. However, this hypothesis is not tested. Hence origin of ‘ ρ ’ class activity in GRS 1915+105 is poorly understood. The similarity of the ρ X-ray class of GRS 1915+105 with the variability observed in IGR J17091-3624 motivated us to perform a detailed analysis of the current outburst of IGR J17091-3624.

In the present work, we have considered all observations of this source between 09 February 2011 and 10 April 2011 with the *RXTE*/PCA and the *SWIFT*/XRT. We analysed both timing and spectral properties of the source after confirming that the contamination from the nearby source IGR J17098-3628 was usually very small. In section 2 we describe our analysis methods. Spectral analysis of the *SWIFT*/XRT show the steepening of powerlaw index when the X-ray flux (0.3-10.0 keV) increased by a factor of ~ 4.5 . A gradual and prominent change in the variability was detected which led to the class transition of the source. The nature of the compact object (in X-ray binaries) plays an important role in selecting spectral model parameters. However, nature of compact object in IGR J17091-3624 is not well determined. Spectra of black hole X-ray binaries (BHXBs) are generally described by a soft X-ray emission from the disk and hard powerlaw emission from corona/base of jet. Using combined *RXTE*/PCA and *INTEGRAL*/IBIS data, Capitanio et al. (2006) found that a single thermal comptonization component (`compTT` in `XSPEC`) or saturated comptonization (`compST` in `Xspec`) or the combination of soft multicolor disk blackbody and hard powerlaw (`diskbb+powerlaw`) are good description of the X-ray spectra of IGR J17091-3624. However, they found the electron temperature in thermal comptonization model was ~ 20 keV, which was less than typical electron temperature of black hole X-ray binary (~ 50 -100 keV)(Zdziarski & Gierliński 2004). The hard X-ray outburst in this system and the large flux of powerlaw spectral component over soft thermal component are commonly seen in BHXB systems. The preliminary spectral data during the recent outburst in 2011 showed that a soft spectral component is necessary to describe the spectrum along with the hard powerlaw component (Del Santo et al. 2011). Section 3 summarizes all results regarding hard state and the hard intermediate state, fast source evolution and transition to a ‘ ρ ’-like class via intermediate variability state, observed in IGR J17091-3624. Finally we have compared the timing and spectral properties of the ‘ ρ ’-like class with the ‘ ρ ’ class characteristics seen in GRS 1915+105 in section 4. We give our conclusion in section 5.

2. Observations and Data Analysis

We analyzed all 34 pointed observations of IGR J17091-3624 made with *RXTE*/PCA between 9 February 2011 (MJD 55601) and 10 April 2011 (MJD 55661). We used archival data for 28 observations from 9 February 2011 to 29 March 2011, and real time data for last six observations. Due to insufficient amount of data and inferior quality, we were unable to extract the background data file for all of the High-Energy X-ray Timing Experiment (HEXTE; Rothschild et al. (1998)) observations. Hence, we used only the *RXTE*/PCA standard-2 science array data and event mode good xenon data for our analysis. Observation details are given in Table 1. We also analyzed three *RXTE*/PCA observations of GRS 1915+105 on 26 May 1997, 03 June 1997 and 22 June 1997 when the sources was in ‘ ρ ’ class. *RXTE*/PCA consists of an array of five proportional counters (PCU0-4) filled with xenon gas, with total effective area of $\sim 6500 \text{ cm}^2$, operating in 2.0-60.0 keV energy range (Jahoda et al. 1996). We used data observed with all xenon layers of PCU2. During the start or the stop of any PCU unit, many observations showed large count rate fluctuations due to the instrument in the lightcurve. To take care of that, we first created xte filter file for each PCA observation and calculated good time interval (GTI) from the exposure time by applying all standard filtering criteria including breakdown events. Calculated values of good time interval are provided in Table 1. Using GTI values of individual observation, we extracted background subtracted light-curve from good xenon data having resolution of 125 micro-sec. As the variability time scale found in light curve is larger than the actual resolution, we used 1s re-binning. Observations with the background subtracted PCA intensity $\geq 15 \text{ cts s}^{-1}\text{PCU}^{-1}$ were considered.

We also analyzed 27 archival data sets of *SWIFT*/XRT between 03 February 2011 and 30 March 2011. The XRT instrument on board *SWIFT* satellite has the effective area is 110 cm^2 at 1.5 keV, the position accuracy is $\sim 5 \text{ arcsec}$ and is operating in 0.2-10.0 keV energy range (Burrows et al. 2005). The typical spectral resolution of this instrument is $\sim 140 \text{ eV}$ at 6.0 keV. To avoid pile-up problem while observing luminous X-ray sources, all observations (except the first one) were performed with Windowed Timing (WT) mode which has time resolution of 1.8 ms and flux limit of $\sim 0.6 \text{ mCrab}$ ($\sim 200 \text{ cts/s}$) (Mineo et al. 2006). For our analysis, we used level 2 cleaned event data which had been extracted from level 1 calibrated data after applying several screening criteria on specific parameters like CCD Temperature, Sun Angle, Elevation Angle etc. For all WT mode data, we assigned grade 0-2 and selected good event with `STATUS==b0`. For each observation, we first extracted the image. Then following the standard procedure for selecting source region as well background region, we extracted source and background lightcurves and spectra separately using `xselect v2.4b` in `FTOOLS 6.10`.

Top panel of Fig. 1 shows that the background-subtracted average *RXTE*/PCA count rate between 2.0-60.0 keV. We found sudden drop in *RXTE*/PCA count rate from $\sim 600 \text{ cts/s/PCU}$ to $\sim 190 \text{ cts/s/PCU}$ after first 14 days of observations. Surprisingly, at the same time, the background-subtracted average *SWIFT*/XRT count rate between 0.3-10.0 keV showed an increase by a factor of ~ 4 . Detailed analysis showed that during first 14 days of observation, IGR J17091-3624 was within the field of view of persistently luminous Z-type neutron star low mass X-ray binary GX

349+2 ($17^h05^m44.49^s$ (R.A. (J2000.0)), $-36^\circ25.38'$ (declination (J2000.0))). As a consequence, very high PCA count rate was observed in first 14 days of observation compared to the rest. Therefore, in our present work, we considered PCA observations from 23 February 2011 onwards (observations falls right to the straight line in the top panel of Fig. 1) to avoid the contamination effect. Further to check possible contamination from IGR J17098-3628, a transient black hole X-ray binary located $9.6'$ away from IGR J17091-3624, we analyzed background-subtracted image from *SWIFT*/XRT in the energy range 0.3-10.0 keV (Fig. 2). The position of IGR J17098-3628 (showed by a circle) is very faint compared to the position of IGR 224 J17091-3624 (showed by a square). For a quantitative measurement, we calculate the count rate separately from the position of IGR J17091-3624 and from the position of IGR J17098-3628. For the energy range 0.3-10.0 keV, their values were 2.023 cts/s and 0.213 cts/s on 3 February 2011. Hence, IGR J17098-3628 has the intensity $\sim 10\%$ of IGR J17091-3624. Since, *RXTE*/PCA could not resolve these sources, it is expected that $\sim 10\%$ contamination effect would be present in *RXTE*/PCA data.

2.1. Timing Analysis

For each PCA observation we created a deadtime corrected and white noise subtracted power density spectrum (PDS) to study different variability features and to track the nature of change occurred in the source with time. The dead time corrections are first applied to the lightcurves. For GoodXenon data, the dead time per event is approximately $10 \mu s$. For details of the procedure, please check *RXTE* cookbook¹. These corrected lightcurves were used to create PDS in 2.0-60.0 keV energy range. To improve the signal-to-noise ratio in the PDS, we used the geometric re-binning of frequency bins of the factor of 1.02^2 . The expected white noise was subtracted from the PDS² and they were normalized such that their square root of integral over the range of frequencies provide fractional rms variability. For same values of bin time and geometric re-binning we also produced PDS from the *SWIFT*/XRT data using background subtracted light-curve between 0.2-10.0 keV energy range. We used same method of normalization. Since one could not compare the 2.0-60.0 keV PDS from the PCA data with 0.2-10.0 keV PDS from *SWIFT*/XRT data, hence we extracted *SWIFT*/XRT PDS for observation dates for which only *SWIFT*/XRT data were available. Several QPO-like features were noticed in the PDS of different *RXTE*/PCA observations. Their approximate characteristics are given in Table 1. Most of the *SWIFT*/XRT PDS were noise dominated or without any feature.

¹http://heasarc.nasa.gov/docs/xte/recipes/pca_deadtime.html

²<http://heasarc.nasa.gov/xanadu/xronos/help/powspec.html>

2.2. Spectral Evolution

The color-color diagram (CD), the hard color vs. soft color plot and the hardness intensity diagram (HID) were created using the PCA Good Xenon data with 1.0 s bin time. The soft color was computed by dividing the background subtracted PCA count rates in the energy band 5.0-12.0 keV by that in the energy band 2.0-5.0 keV. Similarly, the hard color was defined as the ratio of the background subtracted count rate in the energy band 12.0-60.0 keV and 2.0-5.0 keV. X-ray intensity is the background subtracted PCA count rate in 2.0–60.0 keV energy range. Since the channel gain varies from epoch to epoch, we calculated absolute channel ranges corresponding to each of the energy ranges used to calculate soft color, hard color and X-ray intensity for the present epoch. For each *RXTE*/PCA observation, mean count rate (top panel of Fig. 1), and mean value of hard color and soft color have been calculated for a given set of data and their standard deviation values were provided as error (provided in table 1).

2.3. Spectral Fitting

In case of *RXTE*/PCA, we performed the time segmented spectral analysis using GoodXenon data. The details of the analysis is given in section 3.4.1. In case of *SWIFT*/XRT data, we first extracted raw 1D image of the source. Then choosing suitable source region and background region, we extracted source spectrum and background spectrum separately from the cleaned and pointed WT mode event file. We used the latest standard response matrix file (rmf) and auxiliary response file (arf) for WT mode data between 0-2 grade values. We used *XSPEC v 12.6.0* for spectral fitting of *RXTE*/PCA and *SWIFT*/XRT data. Sudden drop in spectral counts with poor signal-to-noise ratio have been observed for lower energy channels of PCA. Similarly very high energy channels are also affected by high background count rate. Hence to maintain uniformity, we used ~ 2.5 -28.0 keV energy spectrum for our spectral fitting.

We have tried different single component models like `diskbb` or `compTT` or `powerlaw` as well as dual component models like `diskbb+powerlaw`, `diskbb+compTT` or `compTT+powerlaw` to fit the source spectra. The reason for selecting and testing different models are greatly discussed in 1. We found that the single *SWIFT*/XRT spectra could be fitted well with a combination of `diskbb` and/or `powerlaw` model. Fitting with the rest of the model combination yielded unacceptably large reduced χ^2 . We used a small Gaussian component at 6.4 keV in order to improve the reduced χ^2 in some observations. To account the effect of absorption by the neutral Hydrogen, all model components were multiplied by a photo-electric absorption model. The Galactic absorption column density at the direction of $17^h 11^m 12.5^s$ (R.A. (J2000.0)), $-36^\circ 24.6'$ (declination (J2000.0)) was calculated as $0.79 \times 10^{22} \text{ cm}^{-2}$. Again from spectral analysis, we found that for all observations, absorption column density varies between 0.82 ± 0.2 and 0.99 ± 0.3 . Thus we kept this value fixed at $0.9 \times 10^{22} \text{ cm}^{-2}$ for all spectral fitting. The unfolded fitted spectra between 2.5-28.0 keV are shown in bottom left panel of Fig. 3 along with its model component and residual. Table 2 shows the fitted

values of different model component parameters.

3. Results

After determining the part of observations which is useful for our present work, we performed the detailed analysis of the combined *RXTE*/PCA and *SWIFT*/XRT data. *SWIFT*/XRT observations of IGR J17091-3624 showed a transition of the source from the low count rate hard state to the high count rate hard state (see top panel of Fig. 1) and a gradual transition in the variability, i.e., from an irregular non variability state, to a regular, repetitive and large variability state. This new variability looked very similar to the unique variability observed during the ‘ ρ ’ class of GRS 1915+105 (Altamirano et al. 2011b). This motivated us to perform a comparative study between these sources. For better distinction of above states, we performed the count rate fractional rms analysis of different observations (by dividing the square root of the variance with the mean count rate) from *RXTE*/PCA which is shown in the bottom panel of Fig. 1. Observations which have fractional rms values less than 3.2 are found to be in hard intermediate state and fractional rms more than 3.2 are found to be in variable state. A few observations showed the transition between hard intermediate state and variable state, and hence described as ‘Intermediate variable state (IVS)’. The details have been discussed below.

3.1. Hard State and Hard intermediate state

From 14 February 2011 to 24 February 2011, a gradual transition in the *SWIFT*/XRT flux between 0.3-10.0 keV was observed in IGR J17091-3624. Initially till 14 February 2011, average *SWIFT*/XRT count rate was ~ 10 cts/s. Then it gradually increased to ~ 45 cts/s on 24 February 2011. To check whether this rise in flux led to any state transition, we analyzed the *SWIFT*/XRT data of 10 February 2011 when the flux is low and 04 March 2011 when the flux is high. Background-subtracted light curve for both observations did not show any specific change in variability (Top left panel of Fig. 3). Secondly, the Leahy normalized power density spectra of both observations show similar spectral shape and the total integrated power between 0.1 Hz and 10.0 Hz are also close to each other (top right panel of Fig. 3). Hence timing properties of the source remain unaffected by the increase of the count rate.

Now to check the spectral behavior of the source during low-flux to the high-flux transition, we did energy spectral analysis of both observations, i.e., 10 February 2011 and 04 March 2011 respectively. We tried different model components the description of which is given thoroughly in § 2.3. While fitting with 1% systematic error, different models described in § 2.3, failed to describe the spectra except `diskbb+powerlaw` model. All of them (like `diskbb`, `compTT`, `diskbb+compTT` etc.) fitted the spectra with unreasonably high reduced χ^2 value (>1.5) while `diskbb+powerlaw` model gives acceptable fit with reduced $\chi^2 \sim 0.85$. This is not so surprising, since most of the BHXB

spectra are well described by the `diskbb+powerlaw` model combinations (Remillard & McClintock 2006). However, we found that disk component is not significant while fitting the spectrum observed on 10 February 2011. A single powerlaw can adequately describe all low flux spectra between 03 February 2011 and 22 February 2011. Bottom panels of Fig. 3 show the unfolded energy spectra, fitted model components and residuals of observations during low flux on 10 February 2011 (left) and during high flux on 04 March 2011 (right). Table 2 show the parameter values of fitted model components during the low flux state and the high flux state respectively. From Table 2, it is clear that all low flux state observations have photon index value less than 1.8 and no disk component is present at the detectable limit of *SWIFT*/XRT. These meet the criteria of a Hard state as defined by Remillard & McClintock (2006). On the other hand, all high flux state observations have powerlaw indices between 2.1 and 2.4. Now spectra with powerlaw index between 2.1 (upper limit for hard state) and 2.4 (lower limit of the Steep Power Law (SPL) state) are defined as a Hard intermediate state (HIMS) by Remillard & McClintock (2006). The increase in powerlaw photon index is first observed on 22 February 2011 using *SWIFT*/XRT (See Table 2). Later we confirm this by performing RXTE/PCA spectral analysis of all observations under consideration. We found that all observations with low flux belong to the hard state while all observations with high flux belong to the HIMS. Our results agree well with spectral parameters obtained by Capitanio et al. (2012) using the joint spectral analysis of *INTEGRAL*/IBIS and *SWIFT*/XRT data. The relatively small difference between our results may be due to their (1) use cutoff powerlaw (where cutoff energy >70 keV, see Table 1 of Capitanio et al. (2012)) (2) different absorption column density (1.1 ± 0.3).

Using *RXTE*/PCA rms normalized power density spectra between 2 mHz and 12 Hz, we found a significant evolution in the QPO frequencies in different observations. Table 1 show that from 26 February 2011 to 6 March 2011, QPO frequency increased from ~ 3.81 Hz to ~ 5.53 Hz. Then it decreased to ~ 5.17 Hz on 10 March 2011. No high frequency QPOs were significantly detected upto 100 Hz.

3.2. Intermediate variable state

During the continuous monitoring of the PCA light curve of IGR J17091-3624, we found a change in the variability pattern from 02 March 2011 to 19 March 2011 (see the top left panel of Fig. 4) in the energy range 2.0-60.0 keV. On 02 March 2011, the source was in hard intermediate state when the light curve was less variable and very similar to the typical light curves seen in canonical BHXBs. On 19 March 2011, the light curve showed a very regular repetitive pattern and high variability (peak count rate $\sim 3-4$ times higher than the count rate at the persistent level). We denoted it by variable state. Observations and average count rate that belonged to the HIMS and variable state were separated by a dashed line in Fig 1.

This transition occurred through some semi-oscillatory intermediate stage on 14 March 2011. The random noisy pattern in the lightcurve of 02 March 2011 seems to take an oscillatory shape on 14 March 2011. Although these intermediate phases are transient but it has been observed couple of

times like on 23 & 24 March 2011, when the source oscillates between the HIMS and variable state. The rms normalized PDS during the intermediate variable state (IVS) showed QPOs in 10–20 mHz frequency range which increased to 20–50 mHz range during variable state. HIMS PDS do not show any such mHz QPO which remarkably distinguish the variable state from the HIMS (Table 1). Interestingly, the HIMS PDS and the IVS PDS share equal source power continuum except a strong QPO at 4.18 Hz during the HIMS whereas the variable state PDS shows very high power with mHz QPO below 0.5 Hz and it drops to noise power continuum before 1 Hz. Fractional rms amplitude of the PDS was found to be 11.6% which is intermediate between 5.8% (HIMS) to 21.4% (variable state) (top right panel of Fig. 4). To trace any change in spectral state during this transition, we plotted in Fig. 4 the HID (bottom left panel) and the CD (bottom right panel). In the HID, the intermediate variable state shows slightly higher flux and larger hardness variability. From the HID, it is seen that the lower limit of the hard color value in the intermediate phase is less than the lower limit of the HIMS. In the CD, the distribution pattern slightly moved towards bottom left corner. However, in both cases, intermediate variable state lie between HIMS and variable state. These results show significant change in the timing properties of the source but not much change in spectral properties. To check this, we performed energy spectral analysis of Intermediate variable state (IVS) on 14 March 2011 between 2.5–30.0 keV. The spectrum can be well fitted by `diskbb` and `powerlaw` model which showed parameter values similar to the HIMS.

3.3. Variable state

The new variable state remained stable for almost 26 days. The recurrent time scale of this variability was found to change with time. Fig. 5 showed the evolution of the source via five *RXTE*/PCA lightcurves from 19 March 2011 to 10 April 2011. On 19 March 2011, the variability timescale of recursive bursts was ~ 41 sec and the burst peak count rate was ~ 2.92 times more than the count rate at minimum level. These bursts have simple profile with slow-rise and fast-decay. As these bursts evolve, flaring frequency increases. On 10 April 2011, the recurrence time scale of the variability became ~ 21 sec. and the burst became more structured. The ratio of burst peak count rate to the persistent level count rate became ~ 3.38 . Careful observation of burst profiles revealed two unique burst structures. (1) Burst profile seen on 31 March, 2011. They have a single peak and the count rate rises slowly (~ 30 sec) to the peak of the burst. (2) Burst profile seen on 03 April, 2011, these bursts are characterized by double peak and show faster rise in count rate (~ 15 -20 sec). Their peak-to-persistent level count rate ratio is ~ 2.84 . This behavior and variation in burst profile structures of the source has so far been seen only in the ‘ ρ ’ class of GRS 1915+105. From the bottom panel of Fig. 1 and Fig. 5, it is clear that variabilities becomes stronger (i.e., higher amplitude of oscillation) and faster (i.e., smaller recurrence time-scale of the burst) with time. From the PDS, we found dual QPO-like features in few observations. For example, QPO features were found at ~ 26.6 mHz and ~ 51.8 mHz on 22 March 2011, and at ~ 24.8 mHz and ~ 49.6 mHz on 29 March 2011, at ~ 37.2 mHz and ~ 75.3 mHz were found on 03 April 2011, at ~ 46.5 mHz and ~ 94.0 mHz were found on 10 April 2011 etc.)(see Table 1). Multiple QPOs were

observed at ~ 24.3 mHz, 45.2 mHz & 70.4 mHz on 30 March 2011 and at ~ 28.1 mHz, 54.5 mHz and 84.6 mHz on 31 March 2011 (see Table 1). Noise components with variable strength were detected in different observations. We also detected QPOs around 8–10 Hz during this state (see Table 1 and upper middle left panel of Figure 9).

In the following section, we explored other properties of the variable state, and compare them with those of GRS 1915+105.

3.3.1. Properties of variable state in comparison to GRS 1915+105

As the variable state in IGR J17091-3624 looks similar to the ‘ ρ ’ class of GRS 1915+105, we make a comparative study between them.

All panels of Fig. 6 showed the 2.0-60.0 keV light curve in both sources. To track the change in variability pattern, we took two observations of variable state in IGR J17091-3624 which show transition from the slow & low flux variability (31 March 11)(top left panel of Fig. 6) to the fast & high flux variability (10 April, 11)(bottom left panel of Fig. 6). Similar transition from the slow & low flux variability (top right panel of Fig. 6) to the fast & high flux variability (bottom right panel of Fig. 6) was observed in GRS 1915+105 on 26 May 1997 and 22 June 1997 respectively. However, it is interesting to observe that the peak count of the bursts in GRS 1915+105 increased significantly while transiting from the slow variability to the fast variability (~ 4000 cts/s/PCU to ~ 5000 cts/s/PCU) while it increased slightly in IGR J17091-3624 during the variable state. This variability in IGR J17091-3624, although repetitive, was irregular, less structured and more quasi-periodic compared to the ‘ ρ ’ class of GRS 1915+105.

Previously a strong anti-correlation between the variability pattern in lightcurve and hardness ratio (defined as the ratio of count rate between 12.0-60.0 keV and 2.0-12.0 keV) was found in the ‘ ρ ’ class of GRS 1915+105 (Yadav et al. 1999). This anti-correlation was also found in the variable state of IGR J17091-3624. Fig. 7 shows the comparative result of anti-correlation found in IGR J17091-3624 on 31 March 11 (top and bottom left panels) and in GRS 1915+105 on 22 June 97 (top and bottom right panels). It is clear that the hardness ratio is higher in IGR J17091-3624 than that observed in GRS 1915+105.

To study the nature of the bursts in details, we studied the rise and the decay profiles for both sources. Left panel of Fig. 8 showed the combined rise profiles of several bursts and combined decay profiles of same bursts in IGR J17091-3624 on 31 March 11. To study the average behavior of rise profiles, we normalized the starting time of each profile to 0 sec. Similarly, to study the average behavior of decay profiles, we normalized the starting time of each profile to 15 sec. We repeated the same procedure for the observation on 22 June 97 of GRS 1915+105 (shown in the right panel of Fig. 8) except for the fact that the starting time of each decay profile was normalized to 70 sec. We fit the combined rise profile with exponential function $f_{rise}(t) = ae^{t/t_{rise}}$ (red continuous line), the combined decay profile with exponential decay function $f_{decay}(t) = ae^{-t/t_{fall}}$ (blue continuous line)

and all profiles with straight line (red and blue dotted line). In case of GRS 1915+105, exponential function fits better than straight line in both rise and decay profile with the significance of $1-1.94 \times 10^{-70}$ and $1-1.31 \times 10^{-38}$ respectively. In IGR J17091-3624, the corresponding significance values were 0.312 and $1-1.99 \times 10^{-4}$ respectively. The slope of the exponential function, for both rise and decay, were found similar in both sources (see Table 3). This indicate that the origin of burst structure might be similar in both sources.

Top panels of Fig. 9 showed that the low frequency (0.1–10.0 Hz) power, QPO strength and the nature of noise components are similar for both sources. White noise subtraction was not applied only for PDS shown in the top panels of Fig. 9. High frequency power disappeared above 1 Hz in case of IGR J17091-3624(top left panel of Fig. 9) but the powerlaw like continuum in GRS 1915+105 continued at higher frequencies along with broad QPO like feature at 8–10 Hz (top right panel of Fig. 9). Harmonics at mHz frequency are seen in both sources. In case of IGR J17091-3624, we have found 8–10 Hz QPO during ‘ ρ ’ like X-ray activity on 25-03-11, 27-03-11, 31-03-11 and 10-04-11 (see Table 1). Upper middle panel of Fig. 9 show 8–10 Hz QPOs for both sources. It is notable that the strength of 8–10 Hz QPOs in IGR J17091-3624 are lower than that observed in GRS 1915+105. Lower middle panels of Fig. 9 show the comparative study of the HIDs between two sources which shows similar general trend but slightly different range in hard color for both sources. For the quantitative measurement of the variability evolution, we considered the PDS of few observations where the first and the last observation were 26 days apart for both sources. During all observations under consideration both sources were in ‘ ρ ’-like class. Bottom left panel of Fig. 9 showed that the fundamental peak in the PDS of IGR J17091-3624 shifted from ~ 12.3 mHz (on 14 March 2011) to ~ 46.8 mHz (on 10 April 2011) in 26 days. While in case of GRS 1915+105, the shift of the fundamental peak in the PDS is from ~ 9.7 mHz (on 26 May 97) to ~ 18.5 mHz (on 22 June 97). Thus the evolution was much faster in IGR J17091-3624 (the change in QPO frequency is ~ 34.5 mHz in 26 days) than GRS 1915+105 (the change in frequency is ~ 8.8 mHz in 26 days). Results on comparative study of both sources are summarized in Table 3.

During 2011 outburst, IGR J17091-3624 evolved from the hard state (upto 22 February, 2011) to the HIMS state and finally to the variable state (similar to ρ class in GRS 1915+105) as X-ray flux increases (see Table 1 of Capitanio et al. (2012) & our Table 2). Detection of accretion disk wind as well as quenching of radio emission during disk dominated state suggests that IGR J17091-3624 is approaching the high soft state (King et al. 2012; Rodriguez et al. 2011b). The HIMS state is characterized by by 3.80–7.08 Hz QPO as well as powerlaw index in the range 2.1–2.4 (Table 1 & 2). During 1997, GRS 1915+105 showed ρ class activity during May-June, 1997 when it evolved from the HIMS state (bright low hard state observed on 26 March, 1997 & 8 May, 1997) to the high soft state during July-August, 1997 (20 July, 1997 & 19 August, 1997)(Rao et al. 2000; Yadav et al. 1999). In GRS 1915+105, HIMS shows QPOs in the range 3.5–4.2 Hz and powerlaw index in the range 2.1–2.5(Rao et al. 2000; Munro et al. 1999). GRS 1915+105 is never seen in the typical low hard state ($\Gamma \leq 1.6$) since its discovery in 1992 but frequently seen in very high state/luminous SPL state where transient radio jets are produced (Mirabel et al. 1998; Eikenberry et al. 1998; Yadav

2006). It may be noted that IGR J17091-3624 is seen in the hard state but not seen in very high state/luminous SPL state. Both these sources show ρ class activities when evolve from the HIMS state. Other BHXBs which show transient radio jets evolve from the quiescent state/low hard state to the very high state/luminous SPL state (Remillard & McClintock 2006). Therefore, IGR J17091-3624 is providing missing link between GRS 1915+105 and other BHXBs.

4. Discussion

We have studied the evolution of the recent X-ray activity in IGR J17091-3624 from 3 February 2011 to 10 April 2011. Initially a hard to hard intermediate state (HIMS) transition was detected by the *SWIFT*/XRT within 0.3–10.0 keV energy range. The hard state is mainly characterized by the low count rate, power-law dominated energy spectrum with the powerlaw index less than 2.1 and the power density spectrum with very high rms. The HIMS is characterized by the high, nonvariable count rate, powerlaw index between 2.1 and 2.4 and both disk component and powerlaw component have significant contribution to the total flux. Few days later, a transition from the HIMS to a regular, repetitive and highly variable state occurred. A few observations between variable state and the HIMS showed low intensity quasi periodic variabilities which we have termed as intermediate variable state. Spectroscopically they are similar to the HIMS. After that, nearly 26 days, the source showed regular, structured, repetitive variabilities similar to the ρ -class, observed only from GRS 1915+105, a Galactic microquasar harboring a black hole of mass $14.0 \pm 4 M_{\odot}$.

In addition to the structural similarity with GRS 1915+105, we found that both sources during ρ class showed similar evolution in the burst structure. With time, burst frequency increases in both sources as well as the ratio of the peak flux to the minimum level flux also increases. In both cases, average rise profile of the burst shows slow exponential rise while average decay profile shows fast decay. Interestingly, we found strong anti-correlation between hardness value and the X-ray flux during variabilities in both sources. The evolution of the burst structure in the HID of both sources is identical. PDS below 1 Hz, showed similar structure. Both sources have strong mHz QPOs sitting on the top of the white noise and both of them showed steep red noise in the PDS along with 8–10 Hz QPOs.

In other BHXBs, transition from the canonical low hard state to the steep power law state via hard intermediate state is commonly observed phenomenon. IGR J17091-3624 also showed transition from the hard state to the HIMS. Spectral properties of the hard state and the HIMS of IGR J17091-3624 also matches with that of other BHXBs. However, GRS 1915+105 is usually seen in the HIMS state (but never seen in the typical low hard state) and it moves to the very high state/luminous SPL state via high soft state. Again, IGR J17091-3624 showed regular repetitive variabilities similar to the ρ class variability observed in GRS 1915+105. This kind of variability has never been observed in any other BHXBs. Thus IGR J17091-3624 showed few properties similar to GRS 1915+105 as well as similar to other BHXBs. Hence it is behaving like a missing link between GRS 1915+105 and other BHXBs.

Although similar observations do not necessarily imply that both sources are of similar type but we found some evidences which tentatively indicate that the central object in IGR J17091-3624 system may be a black hole candidate. One such indication is the detection of type-B QPO at least four times and the detection of type-C QPOs several times. Transient-type Type-B QPOs were seen in few BHXB systems in the frequency range 5–6 Hz around state transition and it has low fractional rms amplitude (2–4 %) and low quality factor ~ 6 and associated with weak red noise (for details, see Soleri et al. (2008)). We detected four QPOs at 5.38, 5.53, 5.39 and 5.17 Hz during the HIMS. Since no PCA data are available during the hard state, hence QPO analysis during hard to HIMS transition is not possible. They have average fractional rms amplitude about 2–3% and quality factor around 4–5 (for details see Table 1). All of them are associated with weak red noise. Thus they satisfied all conditions of type-B QPO. Type-C QPOs are commonly found in BHXB systems and typically found in the frequency range 0.1–15 Hz. They have high rms amplitude (7–12 %), high quality factor (~ 10) and associated with strong flat top noise (for details, see Soleri et al. (2008)). We found several of them in our analysis and type-A QPO was found once at ~ 7.06 Hz (see Table 1). Non-detection of upper and lower kHz QPOs in this source indirectly decreases the chance for the source of being a neutron star. Again the break frequency in the PDS of this source (Lutovinov et al. 2003) further decreases the chance. No type-I X-ray bursts were found in any observations within two months. These bursts unique characteristics of neutron star LMXBs. This gave an indirect evidence that the source might not be a neutron star.

However, we found few dissimilarities between the variable state of IGR J17091-3624 and the ‘ ρ ’ class of GRS 1915+105. They are listed below:

1. The color-color diagram (CD) of the ‘ ρ ’ class showed a loop-like pattern (see Belloni et al. (2000)) while the CD of the variable state in IGR J17091-3624 showed a patchy pattern (see middle right panel of Fig. 4). The X-ray flux in IGR J17091-3624 is lower than that observed in GRS 1915+105.
2. An interesting difference between two systems is that the hardness ratio during ρ class activity is higher (~ 2 times) in IGR J17091-3624 than that observed in GRS 1915+105. Adjustment of black hole mass and its distance may not be sufficient to explain this difference. Peak-to-minimum level count rate ratio for IGR J17091-3624 is ~ 2.9 –3.8. while the value of this ratio is ~ 3.4 –4.3 in case of GRS 1915+105. The absorption column density and contamination from close by source are other parameters which may affect hardness ratio. However, the chance of contamination from close by source is low.
3. Typical low hard state observations where disk emission is not visible, are commonly seen in canonical BHXBs but have never been seen in GRS 1915+105. However, IGR J17091-3624 showed low hard state from 9 March 2011 to 22 March 2011 (see Table 2).
4. A systematic study of the occurrence of different classes during the outburst of GRS 1915+105 (Yadav & Pahari 2011) showed that the ρ class variability eventually arise from the α or ω

class (Pahari & Pal 2010). These are different X-ray classes with different timescale and flux. However, in IGR J17091-3624, the ρ class like activity arises from the HIMS state.

5. The variable state was found stable quasi-continuously for ~ 26 days in IGR J17091-3624, while it was found to be stable for 10–30 days in the GRS 1915+105 although it was not continuous. These observations, in both sources, proved the conclusion of Yadav & Pahari (2011) that ‘ ρ ’ class variability represented very stable X-ray class. The possible reason for prolonged stability of IGR J17091-3624 in the variable state compared to GRS 1915+105 was that to trigger the transition from one variability to another, the disk should cross a critical threshold mass accretion rate. The timescale for attaining this critical mass accretion rate might be longer which prolonged the occurrence of ‘ ρ ’ class in IGR J17091-3624.

Using the radio data, Rodriguez et al. (2011b) found the distance of IGR J17091-3624 to be 10–17 kpc assuming black hole mass to be $10 M_{\odot}$. We used the distance of IGR J17091-3624 to be 14 ± 3 kpc and the compact object mass to be $10 M_{\odot}$ to calculate the mass accretion rate of IGR J17091-3624 relative to the GRS 1915+105. In case of GRS 1915+105, we assume the mass, the distance and the disk inclination angle with respect to observer’s line of sight to be $14.0 \pm 4 M_{\odot}$, 12 ± 2 kpc and 70° respectively. The mass accretion rate at inner disk can be derived using energy conservation law and Virial theorem. Assuming the disk radiation to be blackbody and considering both side of the disk, we get :

$$\dot{m} = 8\pi R_{in,km}^3 \sigma T_{in,keV}^4 / 3GM_{bh} M_{\odot} yr^{-1} \quad (1)$$

where σ is the Boltzmann constant, G is the gravitational constant and $T_{in,keV}$ is the inner disk temperature in keV and $R_{in,km}$ is given by the equation

$$R_{in,km} = \sqrt{N_{diskbb}} \times D_{10,kpc} / \sqrt{\cos i} \quad (2)$$

where N_{diskbb} is the normalization corresponds to the *diskbb* model component in XSPEC, $D_{10,kpc}$ is the distance to the source in the unit of 10 kpc and i is the disk inclination angle with respect to observer’s line of sight. Inserting the equation (2) in (1), we get

$$\dot{m} = \frac{8\pi \sigma T_{in,keV}^4}{3GM} \times (\sqrt{N_{diskbb}} \times D_{10,kpc} / \sqrt{\cos i})^3 \quad (3)$$

The spectral analysis of a stable state (say, ϕ class) in GRS 1915+105 using *RXTE*/PCA provided the average disk temperature of 1.25 ± 0.02 keV and average disk normalization value of 197.34 ± 34.42 . From the HIMS spectral analysis of IGR J17091-3624, we found the value of N_{diskbb} to be 13.87 ± 1.35 and the disk temperature to be 1.24 ± 0.03 (See Table 2). Using this and assuming disk inclination angle (i) to be 70° , we found $\dot{m}_{GRS1915+105} / \dot{m}_{IGRJ17091-3624} \approx 3.78 \pm 0.15$. If we

consider low disk inclination angle, then for $i = 30^\circ$, we found $\dot{m}_{GRS1915+105}/\dot{m}_{IGRJ17091-3624} \approx 18.77 \pm 1.23$. Thus mass accretion rate is always higher in GRS 1915+105 compared to IGR J17091-3624, irrespective of the value of disk inclination angle. This is consistent with high X-ray flux observed in GRS 1915+105 than that seen in IGR J17091-3624 for same distance. We also calculated the relative viscous time-scale of the accretion flow using the following relation:

$$t_{vis}^d = 4.3 \times 10^{-4} \alpha^{-1} \dot{m}_d^{-1} M_{bh}^{-1} R_{in,km}^2 \text{ s} \quad (4)$$

where t_{vis}^d is the dynamic viscous time-scale, α is the viscosity parameter. We considered the value of α to be 0.01 for both sources since this is typical value for most of the BHXBs. Using relation (4) and above parameters, we found the value of $t_{vis|GRS1915+105}^d/t_{vis|IGRJ17091-3624}^d$ to be $\approx 0.676 \pm 0.018$ when the disk inclination angle of IGR J17091-3624 is $\sim 70^\circ$. If the disk inclination angle is 30° , we found $t_{vis|GRS1915+105}^d/t_{vis|IGRJ17091-3624}^d$ to be $\sim 1.281 \pm 0.177$. Thus for a range of inclination angle between 30° and 70° , we found viscous timescale relative to GRS 1915+105 varied between 0.676–1.281. If we assume that ‘ ρ ’-like variability occurred in both sources at same viscous timescale then the disk inclination angle should be very small in IGR J17091-3624.

Thus long term and continuous observation of this source in multi-wavelength band, particularly in hard X-rays as well as soft X-rays would reveal a lot of information regarding the radiation mechanism and accretion flow properties of BHXBs, and help to construct the complete picture of accretion flow around black hole systems by connecting GRS 1915+105 with other canonical BHXB systems.

5. Conclusions

From our analysis of *SWIFT*/XRT and *RXTE*/PCA data during 2011 outburst in IGR J17091-3624, and using the results from comparative study of timing and spectral properties with GRS 1915+105, we conclude following points.

1. We found that IGR J17091-3624 is the only LMXB which showed regular, repetitive and structured variability in the intensity pattern similar to the ρ -type variability seen in GRS 1915+105. Various parameters like burst profile, rise and decay profile, peak-to-minimum flux ratio, harmonics of mHz QPOs, 8–10 Hz QPOs and PDS show remarkable similarity.
2. Several evidences like observation of variability, HID, PDS, power-law dominating spectra etc. provide some indications that the central compact object in IGR J17091-3624 may be a black hole. The detection of type-B and type-C QPOs along with ρ class activity (as seen in GRS 1915+105 which is a black hole) is consistent with the black hole identification of the source.
3. The source showed increase in flux while transiting from hard state to the HIMS. Later a transition from a typical irregular variability state, seen commonly in most of the BHXBs

to the regular, repetitive large variability state, seen only in GRS 1915+105 (ρ -type variability). However, X-ray bursts occur in a state which is spectrally harder than that found in GRS 1915+105. Central black hole mass, its distance, absorption column density etc. may be important to explain the observed hardness ratio but at present we do not know exact answer. It is a topic for future investigations if these parameters or some unknown parameter/mechanism is responsible for higher hardness ratio during ρ class activity in IGR J17091-3624.

4. From Table 1 and bottom panel of Fig. 9, it is clear that we detected several QPOs ranging from few mHz to 10 Hz or so. Such a large range in variability time-scale observed in this source indicate that the accretion disk which may be coupled with the corona, evolved significantly in this source.
5. IGR J17091-3624 is the only source after GRS 1915+105 which show activities like ρ class. In both sources, ρ class activity is observed after the hard intermediate state where disk emission in the energy spectra is visible and contribute significantly to the total flux. GRS 1915+105 never show typical low hard state where disk emission is not visible but IGR J17091-3624 shows low hard state where disk emission is not significant. This result agree well with the low hard state observations of other black hole X-ray binaries. Hence IGR J17091-3624, at certain spectral domain, behave similar to GRS 1915+105 whereas at some other spectral domain, it behaves like other canonical BHXBs. Hence, this source behaves as a missing link between GRS 1915+105 and other canonical BHXBs in understanding their observational dissimilarities, as well as accretion and radiation mechanisms.

6. Acknowledgements

We thank the referee Prof. Ron Remillard for his constructive suggestions/comments. This research has made use of data obtained through the High Energy Astrophysics Science Archive Research Center online service, provided by the NASA/Goddard Space Flight Center and the *SWIFT* data center.

REFERENCES

538

539 Altamirano, D. & Belloni, T. 2012, ApJ, 747, L4

540 Altamirano, D., Linares, M., van der Klis, M., Wijnands, R., Kalamkar, M., Casella, P., Watts, A.
541 & Patruno, A. 2011, Astron. Telegram, 3225, 1

542 Altamirano, D., Belloni, T., Krimm, H. A., Casella, P., Curran, P., Kennea, J. A., Kalamkar, M.
543 & van der Klis, M. 2011, Astron. Telegram, 3230, 1

544 Altamirano, D., Belloni, T., Linares, M., van der Klis, M., Wijnands, R., Curran, P. A., Kalamkar,
545 M., Stiele, H., Motta, S., Muoz-Darias, T., Casella, P., Krimm, H., 2011, ApJ, 742, L17

546 Belloni, T., Klein-Wolt, M., Méndez, M., van der Klis, M. & van Paradijs, J. 2000, A&A, 355, 271

547 Burrows, David N., Hill, J. E., Nousek, J. A., Kennea, J. A., Wells, A., Osborne, J. P., Abbey, A.
548 F., Beardmore, A. et al., 2005, Space Sc. Rev., 120, 165

549 Caballero-García, M. D., Miller, J. M., Trigo, M. Díaz, Kuulkers, E., Fabian, A. C., Mas-Hesse, J.
550 M., Steeghs, D. & van der Klis, M. 2009, ApJ, 692, 1339

551 Capitanio, F., Del Santo, M., Bozzo, E., Ferrigno, C., De Cesare, G., & Paizis, A., 2012, MNRAS,
552 422, 3130

553 Capitanio, F., Tramacere, A., Del Santo, M., Bozzo, E., Watanabe, K., Caballero, I., Chenevez, J.,
554 Paizis, A. et al. 2011, Astron. Telegram, 3159, 1

555 Capitanio, F., Giroletti, M., Molina, M., Bazzano, A., Tarana, A., Kennea, J., Dean, A. J., Hill,
556 A. B. et al. 2009, ApJ, 690, 1621

557 Capitanio, F., Bazzano, A., Ubertini, P., Zdziarski, A. A., Bird, A. J., De Cesare, G., Dean, A. J.,
558 Stephen, J. B. & Tarana, A. 2006, ApJ, 643, 376

559 Castro-Tirado, A. J., Brandt, S., Lund, N., Lapshov, I., Sunyaev, R. A., Shlyapnikov, A. A., Guziy,
560 S. & Pavlenko, E. P. 1994, ApJS, 92, 469

561 Chaty, S., Rahoui, F., Foellmi, C., Tomsick, J. A., Rodriguez, J. & Walter, R. 2008, A&A, 484, 783

562 Del Santo, M., Belloni, T. M., Homan, J., Bazzano, A., Casella, P., Fender, R. P., Gallo, E.,
563 Gehrels, N. et al. 2009, MNRAS, 392, 992

564 Del Santo, M., Kuulkers, E., Bozzo, E., Capitanio, F., Alfonso-Garzon, J., Beckmann, V., Bird, T.,
565 Brandt, S. et al. 2011, Astron. Telegram, 3203, 1

566 Dunn, R. J. H., Fender, R. P., Körding, E. G., Cabanac, C. & Belloni, T. 2008, MNRAS, 387, 545

567 Eikenberry, S. S., Matthews, K., Murphy, T. W., Jr., Nelson, R. W., Morgan, E. H., Remillard, R.
568 A. & Munro, M. 1998, ApJ, 506, L31

- 569 Grebnev, S. A., MolKov, S. & Sunyaev, R. A. 2005, *Astron. Telegram*, 444, 1
- 570 In't Zand, J. J. M., Heise, J., Lowes, P., & Ubertini, P. 2003, *Astron. Telegram*, 160, 1
- 571 Jahoda, K., Swank, J. H., Giles, A. B., Stark, M. J., Strohmayer, T., Zhang, WT., & Morgan, E.
572 H. 1996, *SPIE*, 2808, 59
- 573 Joinet, A., Jourdain, E., Malzac, J., Roques, J. P., Corbel, S., Rodriguez, J. & Kalemci, E. 2007,
574 *ApJ*, 657, 400
- 575 Krimm, H. A. & Kennea, J. A. 2011, *Astron. Telegram*, 3148, 1
- 576 Krimm, H. A., Barthelmy, S. D., Baumgartner, W., Cummings, J., Fenimore, E., Gehrels, N.,
577 Kennea, J. A., Markwardt, C. B. et al. 2011, *Astron. Telegram*, 3144, 1
- 578 King, A. L., Miller, J. M., Raymond, J., Fabian, A. C., Reynolds, C. S., Kallman, T. R., Maitra,
579 D., Cackett, E. M., Rupen, M. P., 2012, *ApJL*, 746, 20
- 580 Kuulkers, E., Lutovinov, A., Parmar, A., Capitanio, F., Mowlavi, N. & Hermsen, W. 2003, *Astron.*
581 *Telegram*, 149, 1
- 582 Lutovinov, A. A., Revnivitsev, M., Molkov, S. & Sunyaev, R. 2005, *A&A*, 430, 997
- 583 Lutovinov, A. A. & Revnivitsev, M. G. 2003, *Astron. Lett.*, 29, 719
- 584 Markoff, S., Nowak, M. A., & Wilms, J. 2005, *ApJ*, 635, 1203
- 585 Massaro, E., Ventura, G., Massa, F., Feroci, M., Mineo, T., Cusumano, G., Casella, P. & Belloni,
586 T. 2010, *A&A*, 513, 21
- 587 Miller, J. M. 2007, *ARA&A*, 45, 441
- 588 Mineo, T., Romano, P., Mangano, V., Moretti, A., Cusumano, G., La Parola, V., Troja, E.,
589 Campana, S. et al., 2006, *Nuovo Cimento B*, 121, 1521
- 590 Mirabel, I. F., Dhawan, V., Chaty, S., Rodriguez, L. F., Marti, J., Robinson, C. R., Swank, J., &
591 Geballe, T., 1998, *A&A*, 330, L9
- 592 Mirabel, I. F. & Rodriguez, L. F. 1994, *Nature*, 371, 46
- 593 Munoz, M. P., Morgan, E. H. & Remillard, R. A., 1999, *ApJ*, 527, 321
- 594 Muñoz-Darias, T., Casares, J., & Martínez-Pais, I. G. 2008, *MNRAS*, 385, 2205
- 595 Pahari, M., Bhattacharyya, S., Yadav, J. S. & Pandey, S. K., 2011, *MNRAS*, 422, L87
- 596 Pahari, M., Bhattacharyya, S. & Yadav, J. S. 2011, *Astron. Telegram*, 3266, 1
- 597 Pahari, M. & Pal, S. 2010, *MNRAS*, 409, 903

- 598 Pandey, M., Manchanda, R. K., Rao, A. P. & Durouchoux, P. & Chandra, C. H. 2006, A&A, 447,
599 525
- 600 Paul, B., Agrawal, P. C., Rao, A. R., Vahia, M. N., Yadav, J. S., Marar, T. M. K., Seetha, S. &
601 Kasturirangan, K. 1998, A&AS, 128, 145
- 602 Rao, A. R., Yadav, J. S. & Paul, B., 2000, ApJ, 544, 443
- 603 Remillard, R. A. & McClintock, J. E., 2006, ARA&A, 44, 49
- 604 Rodriguez, J., Corbel, S., Tomsick, J. A., Paizis, A. & Kuulkers, E. 2011a, Astron. Telegram, 3168,
605 1 F
- 606 Rodriguez, J., Corbel, S., Caballero, I., Tomsick, J. A., Tzioumis, T., Paizis, A., Cadolle, Bel M.,
607 & Kuulkers, E., 2011b, A&A, 533, L4
- 608 Rothschild, R. E., Blanco, P. R., Gruber, D. E., Heindl, W. A., MacDonald, D. R., Marsden, D.
609 C., Pelling, M. R., Wayne, L. R. & Hink, P. L. 1998, ApJ, 496, 538
- 610 Rupen, M. P., Mioduszewski, A. J. & Dhawan, V. 2003, Astron. Telegram, 152, 1
- 611 Shaposhnikov, Nikolai 2011, Astron. Telegram, 3179, 1
- 612 Soleri, P., Belloni, T. & Casella, P. 2008, MNRAS, 383, 1089
- 613 Sunyaev, R. & Revnivtsev, M., 2000, A&A, 358, 617
- 614 Taam, R. E., Xingming, C. & Swank, J., E. 1997, APJ, 485, L83
- 615 Tingay, S. J., Jauncey, D. L., Preston, R. A., Reynolds, J. E., Meier, D. L., Murphy, D. W.,
616 Tzioumis, A. K., McKay, D. J. et al. 1995, Nature, 374, 141
- 617 Yadav, J. S., Rao, A. R., Agrawal, P. C., Paul, B., Seetha, S. & Kasturirangan, K. 1999, ApJ, 517,
618 935
- 619 Yadav, J. S., 2001, ApJ, 548, 876
- 620 Yadav, J. S., 2006, ApJ, 646, 385
- 621 Yadav, J. S., & Pahari, M. 2011 under publication
- 622 Zdziarski, A. A. & Gierliński, M. 2004, Prog. Theor. Phys. Suppl., 155, 99

Table 1: Observational details of IGR J17091-3624 using *RXTE*/PCA and/or *SWIFT*/XRT data during 2011 outburst. HIMS & IVS stand for Hard intermediate state and Intermediate variable state respectively

Observation date (DD-MM-YY)	MJD	Instrument	Observation ID	Good time interval (sec)	Average soft color	Average hard color	lightcurve type and PDS features
03-02-11	55595.90	XRT(PC)	00031920001	983.6	–	–	non-variable, low flux and noise dominated (hard)
09-02-11	55601.06	XRT(WT)	00031921005	1467.4	–	–	low variability, low flux and noise dominated (hard)
10-02-11	55602.58	XRT(WT)	00031921006	2200.4	–	–	low variability, low flux and noise dominated (hard)
12-02-11	55604.21	XRT(WT)	00031921008	2198.1	–	–	low variability, low flux and noise dominated (hard)
13-02-11	55605.21	XRT(WT)	00031921009	2151.2	–	–	low variability, low flux and noise dominated (hard)
14-02-11	55606.16	XRT(WT)	00031921010	1877.6	–	–	low variability, low flux and noise dominated (hard)
15-02-11	55607.23	XRT(WT)	00031921011	2101.6	–	–	low variability, low flux and noise dominated (hard)
16-02-11	55608.23	XRT(WT)	00031921012	2182.3	–	–	low variability, low flux and noise dominated (hard)
18-02-11	55610.17	XRT(WT)	00031921013	2176.5	–	–	low variability, low flux and noise dominated (hard)
20-02-11	55612.25	XRT(WT)	00031921014	2104.2	–	–	low variability, low flux and noise dominated (hard)
22-02-11	55614.19	XRT(WT)	00031921015	2050.2	–	–	low variability, increased flux and noise dominated (hard)
23-02-11	55615.99	PCA	96065-03-01-03	3184.4	0.731±0.013	0.369±0.021	~ low variable, high flux and 4.29 Hz strong QPO feature with weak red noise noticed (HIMS)
24-02-11	55616.25	XRT(WT)	00031921016	1065.6	–	–	high flux and medium variability (HIMS)
26-02-11	55619.01	PCA	96065-03-02-00	1712.2	0.754±0.005	0.409±0.019	~ high irregular variability, high flux and 3.81 Hz strong QPO feature with weak white noise noticed (HIMS)
02-03-11	55622.59	PCA	96420-01-01-00	3744.3	0.724±0.037	0.390±0.078	~ low variability, high flux and 4.18 Hz strong QPO feature with weak white noise noticed (HIMS)
	55622.52	XRT(WT)	00031921018	2340.6	–	–	
03-03-11	55623.28	PCA	96420-01-01-01	2064.5	0.684±0.034	0.364±0.023	~ 4.41 Hz & 9.07 Hz QPO feature and
	55623.86	PCA	96420-01-01-02	6944.4	0.659±0.026	0.385±0.026	~ 4.65 Hz strong QPO feature with weak white noise noticed; high irregular variability & high flux (HIMS)
	55623.29	XRT(WT)	00031921019	971.4	–	–	
04-03-11	55624.56	PCA	96420-01-02-00	1584.2	0.623±0.028	0.327±0.007	~ 5.38 Hz strong QPO feature with weak red noise noticed; low variability, low flux and noise dominated (HIMS)
	55624.37	XRT(WT)	00031921020	2289.4	–	–	
06-03-11	55626.39	PCA	96420-01-02-01	65.5	0.665±0.033	0.349±0.014	~ 5.53 Hz QPO feature with weak red noise noticed; low variability, low flux and noise dominated (HIMS)
07-03-11	55627.62	XRT(WT)	00031921021	2075.7	–	–	low variability, high flux and noise dominated (HIMS)
08-03-11	55628.47	PCA	96420-01-02-02	3202.2	0.643±0.014	0.356±0.005	~ 5.39 Hz QPO feature with weak red noise noticed; low variability, low flux and noise dominated (HIMS)
	55628.23	XRT(WT)	00031921022	1704.1	–	–	
10-03-11	55630.84	PCA	96420-01-02-03	1648.8	0.669±0.019	0.371±0.038	~ 5.17 Hz strong QPO feature with weak red noise noticed; low variability, low flux and noise dominated (HIMS)
	55630.16	XRT(WT)	00031921023	1401.5	–	–	
12-03-11	55632.54	PCA	96420-01-03-00	1520.4	0.626±0.023	0.328±0.024	7.06 Hz QPO feature with weak red noise noticed; irregular variability, high flux and noise dominated (HIMS)
	55632.73	XRT(WT)	00031921024	2182.3	–	–	
13-03-11	55633.24	XRT(WT)	00031921025	2009.8	–	–	weak red noise noticed; irregular variability, high flux and noise dominated (HIMS)
14-03-11	55634.72	PCA	96420-01-03-01	3344.2	0.532±0.022	0.282±0.056	~12.4 mHz and ~2.59 Hz QPO features with very weak red noise noticed; variability become regular and repetitive (IVS)
15-03-11	55635.65	XRT(WT)	00031921026	1481.2	–	–	regular variability and high flux noticed (IVS)
18-03-11	55638.54	XRT(WT)	00031921029	2164.6	–	–	~ 14.6 mHz QPO feature noticed low variability & noise dominated (IVS)
19-03-11	55639.71	PCA	96420-01-04-00	2752.3	0.502±0.007	0.212±0.016	~ 30.7 mHz strong QPO feature with strong red noise noticed (ρ)
	55639.67	XRT(WT)	00031921028	2631.5	–	–	
20-03-11	55640.47	XRT(WT)	00031921030	2352.5	–	–	~ 30.2 mHz strong QPO with red noise noticed (ρ)

Note. — Continuation of Table 1 ...

Observation date (DD-MM-YY)	MJD	Instrument	Observation ID	Good time interval (sec)	Average soft color	Average hard color	lightcurve type and PDS features
22-03-11	55642.20	PCA	96420-01-04-02	2976.4	0.539±0.005	0.294±0.089	~26.6 mHz and ~51.8 mHz QPO feature with strong red noise noticed (ρ)
	55642.35	XRT(WT)	00031921031	2260.3	–	–	
23-03-11	55643.78	PCA	96420-01-04-01	1152.4	0.551±0.112	0.325±0.030	~ 12.3 mHz strong QPO feature with weak red noise noticed (ρ)
	55643.25	XRT(WT)	00031921033	643.5	–	–	
24-03-11	55644.75	PCA	96420-01-04-03	2752.8	0.571±0.028	0.334±0.043	~ 14.4 mHz & 8.06 Hz strong QPO feature with strong peaked noise at 0.06 Hz noticed; quasi regular, low variability (IVS)
25-03-11	55645.86	PCA	96420-01-05-02	3312.3	0.576±0.013	0.371±0.004	Weak red noise and a tentative QPO feature at ~ 6.98 Hz noticed quasi-regular, low variability (IVS)
26-03-11	55646.89	XRT(WT)	00031921034	2160.1	–	–	~ 15.1 mHz QPO feature is noticed (ρ)
27-03-11	55648.01	PCA	96420-01-05-00	32990.4	0.522±0.037	0.272±0.027	~ 24.5 mHz & 8.03 Hz strong QPO feature with weak red noise noticed (ρ)
29-03-11	55649.06	PCA	96420-01-05-03	2640.3	0.546±0.009	0.331±0.023	~24.8 mHz & ~49.6 mHz QPO feature with weak red noise noticed (ρ)
30-03-11	55650.98	PCA	96420-01-05-01	2304.5	0.502±0.009	0.279±0.019	Weak red noise noticed & QPO feature at ~ 24.3 mHz, 45.2 mHz & 70.4 mHz is found (XRT)(ρ)
	55650.74	XRT(WT)	00031921036	331.65	–	–	
31-03-11	55651.88	PCA	96420-01-05-04	3968.1	0.513±0.024	0.345±0.043	QPO features at 28.1 mHz, 54.5 mHz, 84.6 mHz and 9.04 Hz are found with weak red noise (ρ)
02-04-11	55653.70	PCA	96420-01-06-00	3488.7	0.502±0.019	0.298±0.008	Twin peak QPO like feature at 30.7 mHz & 37.1 mHz and strong QPO at 68.7 mHz with strong red noise noticed (ρ)
03-04-11	55654.89	PCA	96420-01-06-01	6112.3	0.532±0.008	0.312±0.037	QPO features at ~37.2 mHz, 75.3 mHz and ~8.06 Hz with strong red noise noticed (ρ)
05-04-11	55656.71	PCA	96420-01-06-02	5136.3	0.540±0.010	0.275±0.036	QPO feature at ~40.4 mHz and strong BLN feature noticed (ρ)
10-04-11	55661.75	PCA	D6308-17-19-06R	3376.6	0.576±0.009	0.283±0.027	QPO features at ~46.5 mHz, ~94.0 mHz and ~8.05 Hz QPO features are noticed with strong red noise (ρ)

Table 2: Best fit parameters (with 1σ error bars) obtained by fitting the hard state and hard intermediate state spectra of IGR J17019-3624 with the **powerlaw** and the **diskbb+powerlaw** model respectively.

Instrument used	Observation ID	Date (DD-MM-YY)	state/class	Γ	kT_{in} (keV)	N_{diskbb}	Flux _{total}	Flux _{powerlaw}	Flux _{diskbb}	χ^2/dof
XRT	00031921005	09-02-11	Hard	$1.66^{+0.05}_{-0.04}$	—	—	0.601	—	—	657.98/632
XRT	00031921006	10-02-11	Hard	$1.75^{+0.05}_{-0.04}$	—	—	0.452	—	—	473.58/632
XRT	00031921008	12-02-11	Hard	$1.63^{+0.03}_{-0.03}$	—	—	0.872	—	—	728.57/632
XRT	00031921009	13-02-11	Hard	$1.69^{+0.03}_{-0.04}$	—	—	0.982	—	—	667.64/632
XRT	00031921010	14-02-11	Hard	$1.73^{+0.04}_{-0.05}$	—	—	0.705	—	—	694.01/632
XRT	00031921011	15-02-11	Hard	$1.67^{+0.03}_{-0.04}$	—	—	0.951	—	—	726.74/632
XRT	00031921012	16-02-11	Hard	$1.62^{+0.03}_{-0.03}$	—	—	1.104	—	—	529.34/632
XRT	00031921013	18-02-11	Hard	$1.66^{+0.03}_{-0.04}$	—	—	1.035	—	—	486.28/632
XRT	00031921014	20-02-11	Hard	$1.79^{+0.04}_{-0.05}$	—	—	0.980	—	—	509.43/632
XRT	00031921015	22-02-11	Hard	$2.22^{+0.07}_{-0.05}$	—	—	2.472	—	—	495.40/632
PCA	96065-03-01-03	23-02-11	HIMS	$2.29^{+0.03}_{-0.03}$	$1.10^{+0.04}_{-0.06}$	$6.43^{+2.42}_{-1.45}$	0.791	0.685	0.106	35.12/42
PCA	96065-03-02-00	26-02-11	HIMS	$2.38^{+0.04}_{-0.07}$	$0.93^{+0.11}_{-0.06}$	$11.50^{+4.30}_{-5.50}$	0.675	0.597	0.078	43.59/42
PCA	96420-01-01-00	02-03-11	HIMS	$2.22^{+0.02}_{-0.03}$	$1.10^{+0.06}_{-0.04}$	$2.69^{+0.76}_{-0.52}$	0.470	0.427	0.043	44.52/42
PCA	96420-01-01-01	03-03-11	HIMS	$2.30^{+0.08}_{-0.03}$	$1.14^{+0.04}_{-0.03}$	$4.36^{+0.56}_{-0.48}$	0.492	0.402	0.09	34.42/42
PCA	96420-01-01-02	03-03-11	HIMS	$2.41^{+0.04}_{-0.03}$	$0.82^{+0.10}_{-0.09}$	$6.08^{+3.25}_{-2.46}$	0.350	0.329	0.021	40.78/42
PCA	96420-01-02-00	04-03-11	HIMS	$2.39^{+0.05}_{-0.06}$	$1.23^{+0.03}_{-0.03}$	$12.30^{+1.93}_{-1.95}$	1.812	1.480	0.330	31.89/42
PCA	96420-01-02-01	06-03-11	HIMS	$2.44^{+0.05}_{-0.06}$	$1.15^{+0.16}_{-0.12}$	$16.30^{+5.35}_{-8.36}$	1.828	1.503	0.33	33.58/42
PCA	96420-01-02-02	08-03-11	HIMS	$2.34^{+0.04}_{-0.03}$	$1.24^{+0.02}_{-0.03}$	$13.87^{+1.35}_{-1.34}$	1.765	1.360	0.405	40.75/42
PCA	96420-01-02-03	10-03-11	HIMS	$2.39^{+0.05}_{-0.06}$	$1.23^{+0.03}_{-0.04}$	$10.97^{+1.92}_{-1.93}$	1.714	1.422	0.29	41.17/42
PCA	96420-01-03-00	12-03-11	HIMS	$2.47^{+0.03}_{-0.06}$	$0.89^{+0.08}_{-0.07}$	$4.47^{+1.15}_{-0.85}$	0.305	0.281	0.024	42.12/42

Note. — Γ is the power-law index, $N_{powerlaw}$ is the power-law normalization, kT_{in} is temperature of the inner disk edge in units of keV and N_{diskbb} is the disk blackbody model normalization. Flux_{total} is the total flux, Flux_{diskbb} is the flux of the disk component and Flux_{powerlaw} is the flux of the power-law component. All the fluxes are calculated in the energy range 2.0-60.0 keV for combined PCA and *SWIFT*/XRT spectra and 0.3-10.0 keV for *SWIFT*/XRT spectra only. Fluxes are given in a unit of 10^{-9} ergs/s/cm².

Table 3: Summary of Comparative study of some characteristic parameters of IGR J17091-3624 and GRS 1915+105.

Characteristic parameters	IGR J17091-3624 (variable state)	GRS 1915+105 (‘ ρ ’ class)
Oscillation timescale	$\sim 20 \text{ s} - 50 \text{ s}$	$\sim 40 \text{ s} - 110 \text{ s}$
Change in timescale	increases with time $\sim 1.32 \text{ mHz/day}$	increases with time $\sim 0.36 \text{ mHz/day}$
Peak to minimum flux ratio	$\sim 2.91 - 3.82$	$\sim 3.38 - 4.28$
X-ray flux and hard color relation	strong anti-correlation found	strong anti-correlation found
Variability pattern (fitting with $f(t)=ae^{t/t_i}$)	slow exponential rise ($t_i=t_{rise} \sim 14.67$) fast decay ($t_i=t_{fall} \sim -3.62$)	slow exponential rise ($t_i=t_{rise} \sim 13.68$) fast decay ($t_i=t_{fall} \sim -2.48$)
QPOs	28.1 mHz, 54.5 mHz (on 31 Mar. 11) 37.2 mHz, 75.3 mHz (on 03 Apr. 11) 46.5 mHz, 94.0 mHz (on 10 Apr. 11) etc.	9.7 mHz & 19.2 mHz (on 26 May 97) 12.1 mHz & 24.3 mHz (on 03 Jun. 97) 18.5 mHz, 37.9 mHz (on 22 Jun. 97)

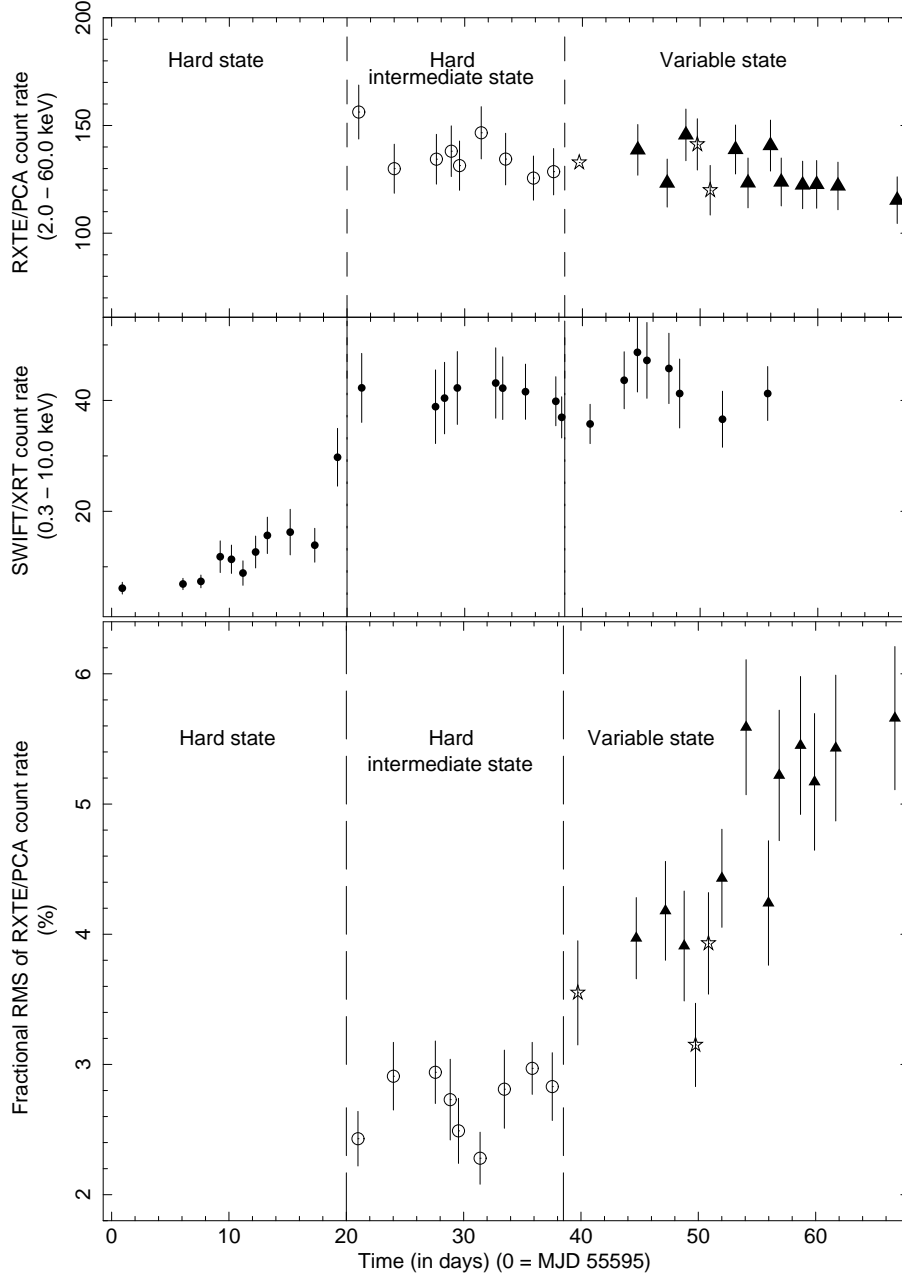


Fig. 1.— Overall nature of 2011 outburst of IGR J17091-3624. *Top panel:* plot of background-subtracted *RXTE*/PCA average count rate between 2.0–60.0 keV with time, *middle panel:* simultaneous plot of background-subtracted *SWIFT*/XRT average count rate between 0.3–10.0 keV with time, *Bottom panel:* fractional RMS values of *RXTE*/PCA count rate as observed during hard intermediate state and variable state. Due to contamination, *RXTE*/PCA has no observation when the source was in hard state. Vertical lines separate the hard state, hard intermediate state and the variable state. Intermediate variable states are shown by stars.

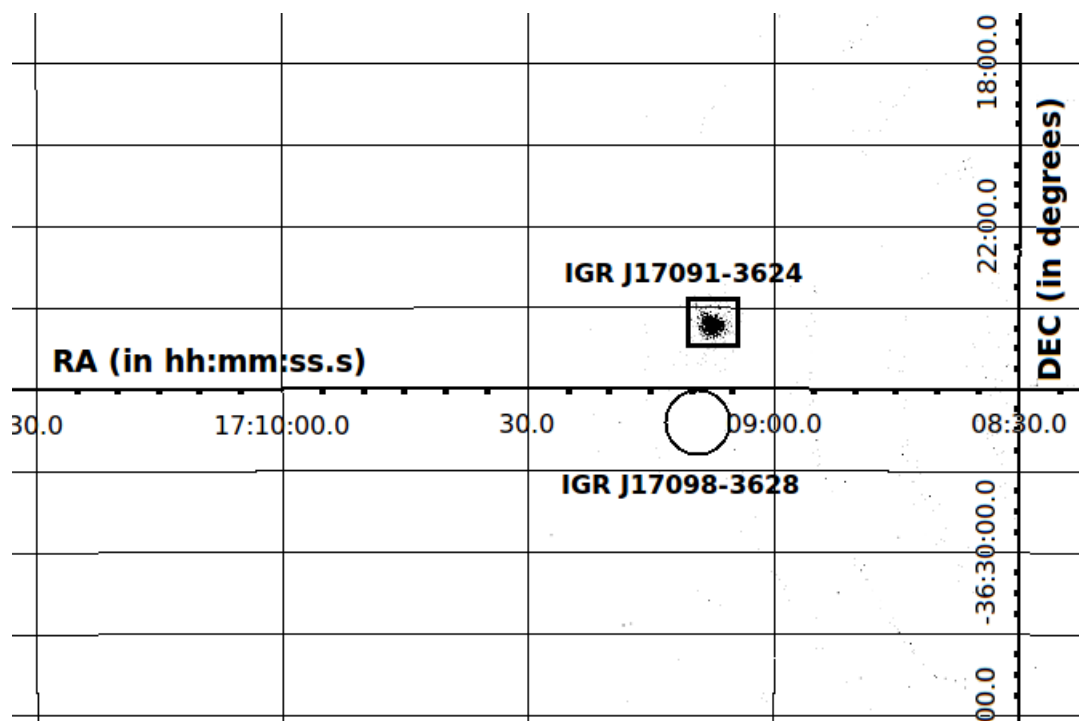


Fig. 2.— 0.3-10.0 keV filtered image of IGR J17091-3624 taken by the *SWIFT*/XRT in the photon counting mode on 03 February 11.

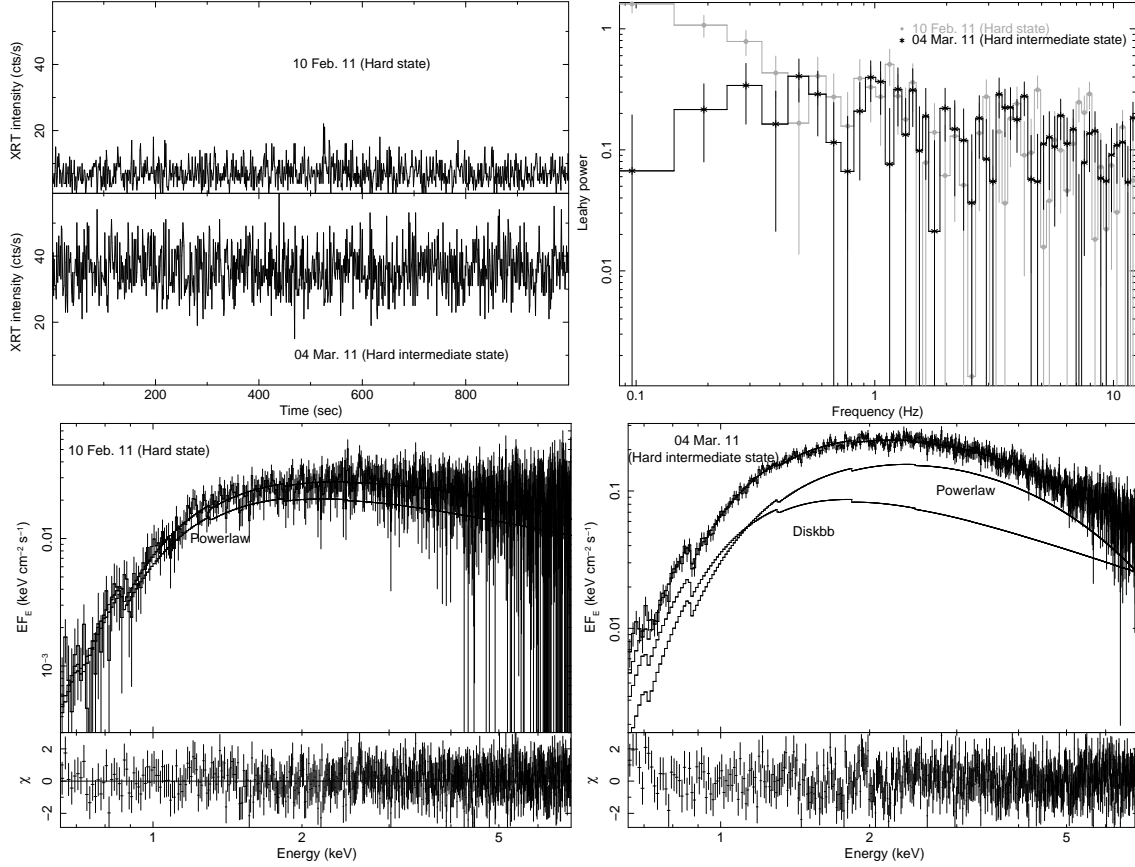


Fig. 3.— Result from *SWIFT*/XRT observations of IGR J17091-3624 during the transition from the hard state to the hard intermediate state. *Top left panel*: 0.3-10.0 keV background-subtracted light curves of the hard state and the hard intermediate state. *Top right panel*: 0.3-10.0 keV rms normalized power density spectrum of the hard state and the hard intermediate state. *Bottom left panel*: 0.6-7.2 keV unfolded energy spectrum, fitted model component (`powerlaw`) and residuals of the hard state. *Bottom right panel*: 0.6-7.2 keV unfolded energy spectrum, fitted model components (`diskbb` and `powerlaw`) and residuals of the hard intermediate state.

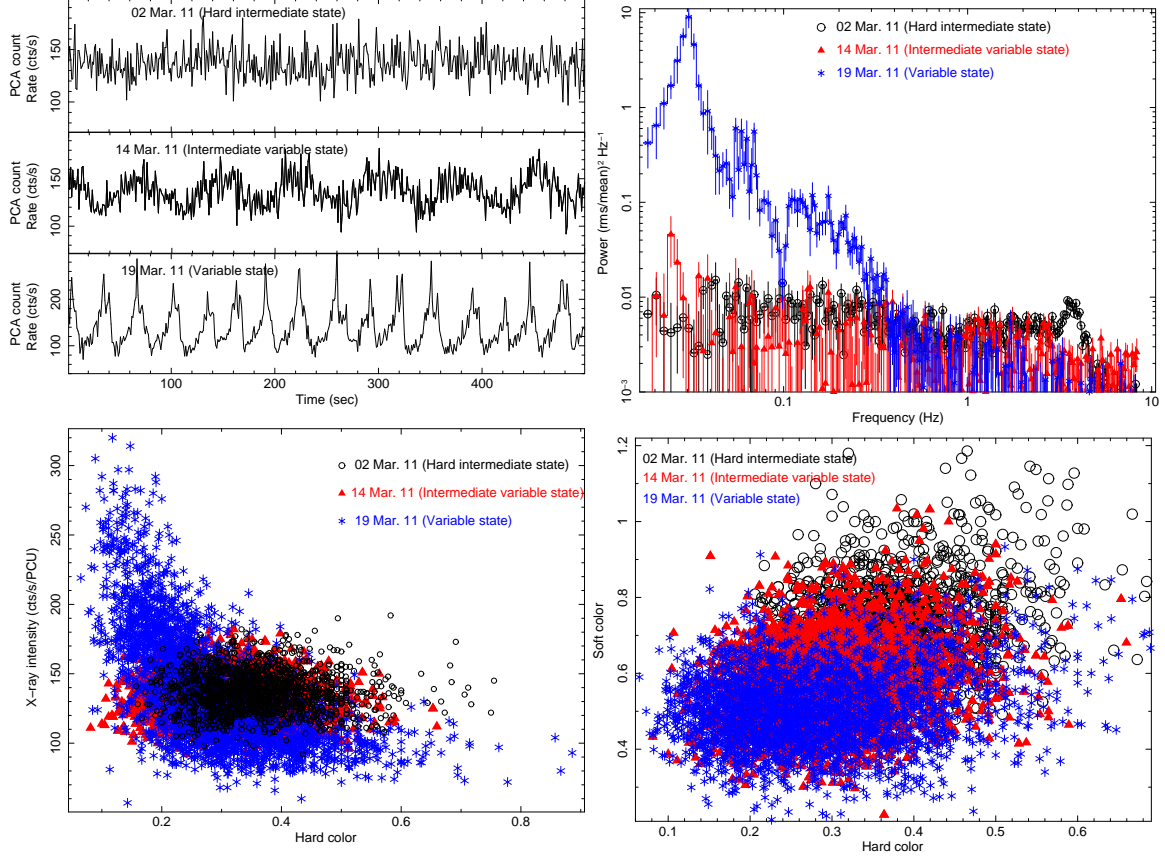


Fig. 4.— Result from observations during transition from low-variability class (hard intermediate state) to high variability class (variable state) via transition class (transition state) of IGR J17091-3624. *Top left panel:* 2.0-60.0 keV *RXTE*/PCA light curves of three types of classes. *Top right panel:* 2.0-60.0 keV *RXTE*/PCA rms normalized power density spectrum of three types of classes. *Bottom left panel:* evolution of classes from hard intermediate state to variable state in the Hardness Intensity Diagram. *Bottom right panel:* evolution of classes from hard intermediate state to variable state in the color color Diagram.

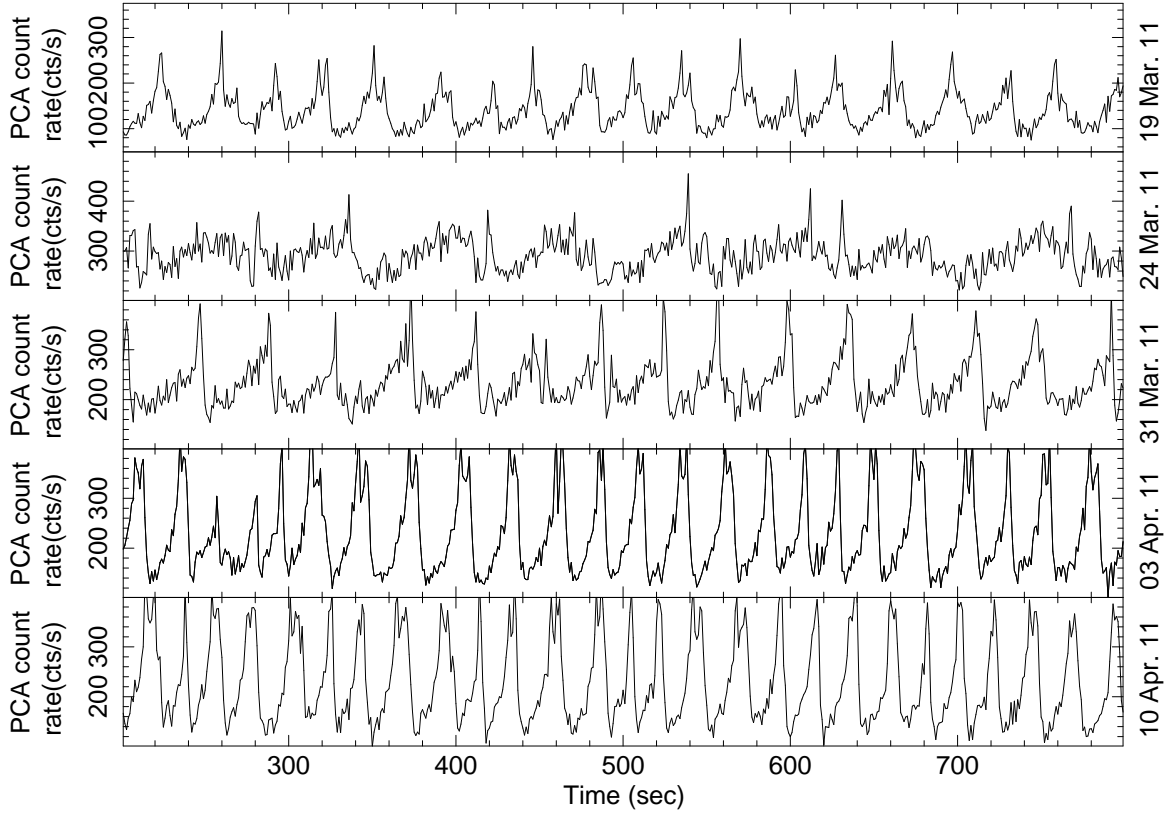


Fig. 5.— Evolution of variability pattern during variable state in IGR J17091-3624. All 5 panels show 2.0-60.0 keV background-subtracted PCA light curve for five different observations from 19 March 11 to 10 April 11 with 1s bintime.

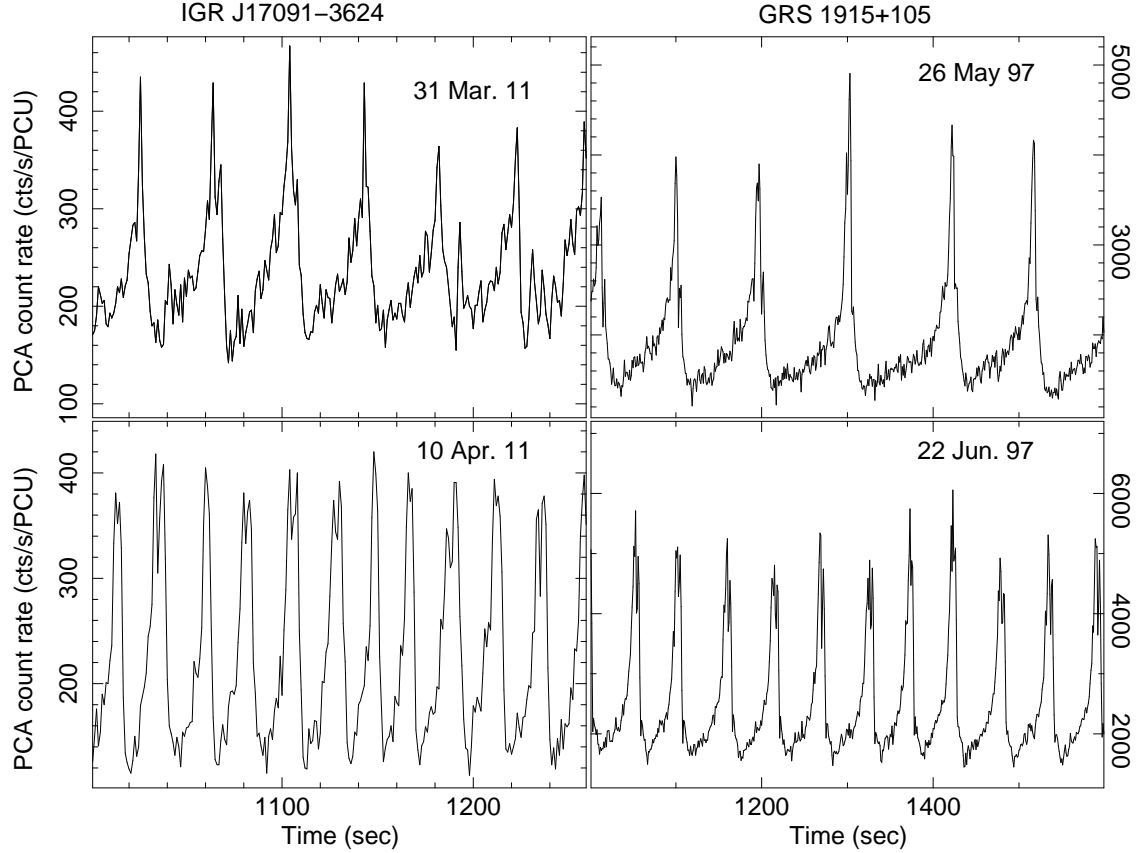


Fig. 6.— Comparative study between the variable state variability class of IGR J17091-3624 and the ‘ ρ ’ class of GRS 1915+105. The left panel figures correspond to 2.0-60.0 keV *RXTE*/PCA lightcurve of IGR J17091-3624 on 31 March 11 (top) and 10 April 11 (bottom) and the right panel figures corresponds to 2.0-60.0 keV *RXTE*/PCA lightcurve of GRS 1915+105 on 26 May 97 (top) and 22 June 97 (bottom). Decrease in variability timescale with time was noticed in both sources.

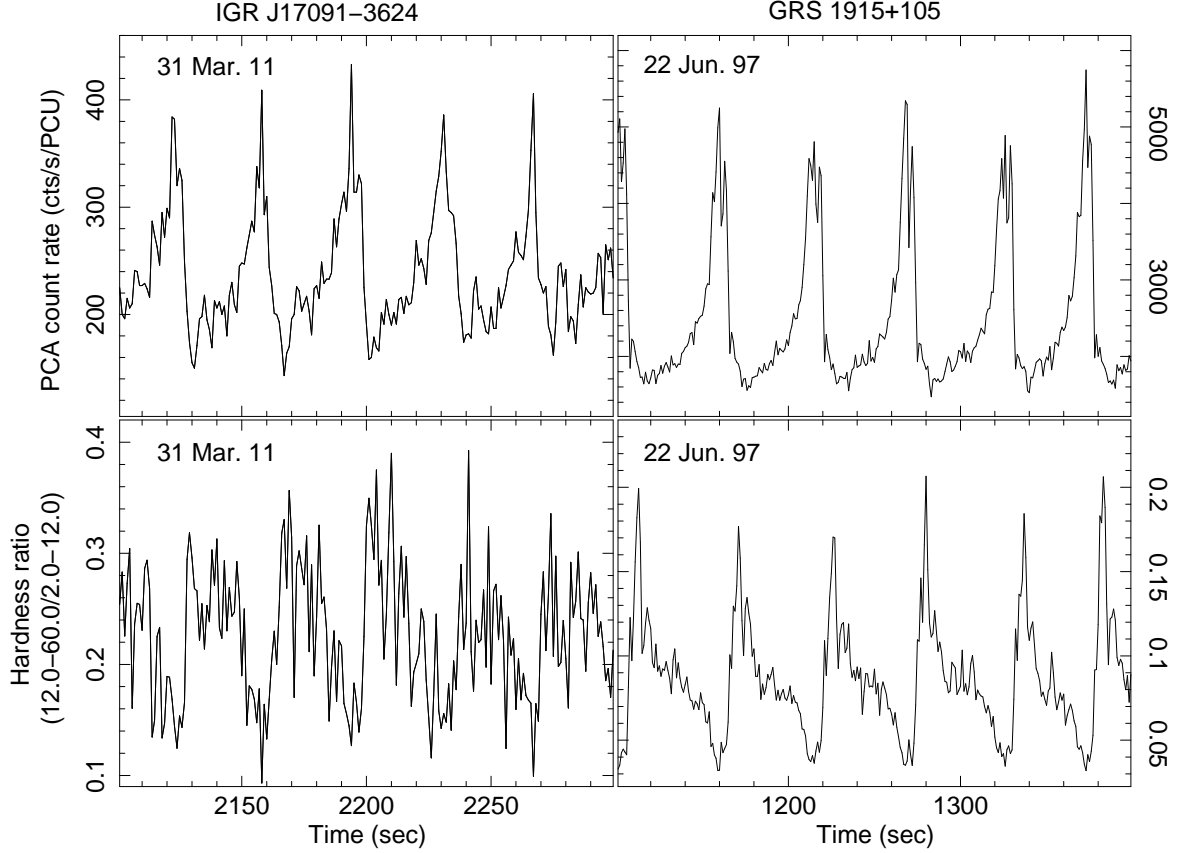


Fig. 7.— Comparative study between the variable state variability class of IGR J17091-3624 and the ‘ ρ ’ class of GRS 1915+105. Top panels show the 2.0-60.0 keV *RXTE*/PCA lightcurve of IGR J17091-3624 (left) and GRS 1915+105 (right). Bottom panels show the plot of hardness ratio (defined as the ratio of *RXTE*/PCA count rate between 12.0-60.0 keV and 2.0-12.0 keV) with time for IGR J17091-3624 (left) & GRS 1915+105 (right). Strong anti correlation between X-ray flux and hardness ratio was found in both sources.

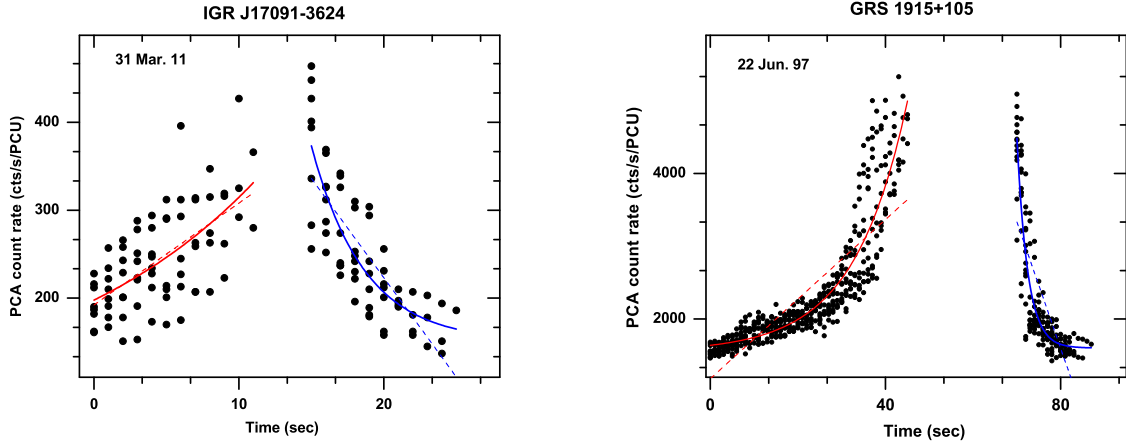


Fig. 8.— Comparative study between the variable state variability class of IGR J17091-3624 and the ‘ p ’ class of GRS 1915+105. *Left panel:* combined rise profile (left) and decay profile (right) of several bursts in IGR J17091-3624. Start of all rise profiles are normalized to 0 sec and start of all decay profiles are normalized to 15 sec. An exponential growth function ($ae^{x/t}$) fitted the rise profile better than a straight line with the significance of 0.312. An exponential decay function ($ae^{-x/t}$) fitted the decay profile better than a straight line with the significance of $1-1.99 \times 10^{-4}$. *Right panel:* combined rise profile (left) and decay profile (right) of several bursts in GRS 1915+105. Start of all rise profiles are normalized to 0 sec and start of all decay profiles are normalized to 70 sec. An exponential growth function ($ae^{x/t}$) fitted the rise profile better than a straight line with the significance of $1-1.94 \times 10^{-70}$. An exponential decay function ($ae^{-x/t}$) fitted the decay profile better than a straight line with the significance of $1-1.31 \times 10^{-38}$.

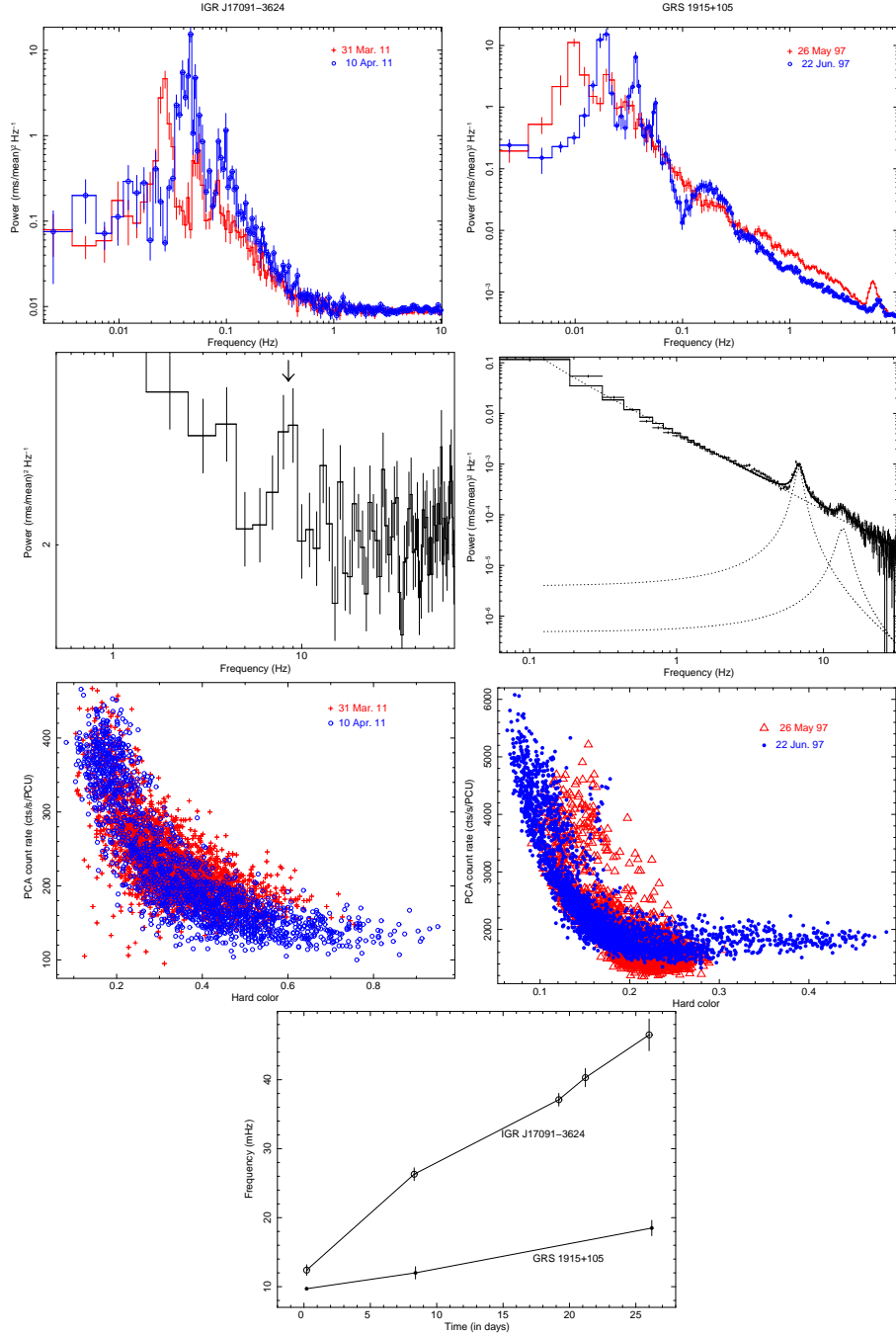


Fig. 9.— All left panel figures correspond to IGR J17091-3624 and all right panel figures correspond to GRS 1915+105. *Top panels:* 2.0-60.0 keV *RXTE*/PCA rms normalized power density spectra. *Upper Middle panels:* Typical 8-10 Hz QPO in the PDS. *Lower Middle panels:* Hardness Intensity Diagrams for both sources for the same definitions of hard color and intensity. Both panels show that both sources evolved in a similar way in the PDS as well as in HIDs as the variability timescale decreases. *Bottom panel:* Evolutions of the characteristic frequencies of the variable state of IGR J17091-3624 (empty circles) and the ρ class of GRS 1915+105 (filled circles). In case of IGR J17091-3624, the time zero in x-axis corresponds to MJD 55635.37, and in case of GRS 1915+105, the time zero in x-axis corresponds to MJD 50594.49. This panel displays that within the same timescale of observations, IGR J17091-3624 shows faster evolution of the variability frequency compared to the ‘ ρ ’ class frequency of GRS 1915+105.